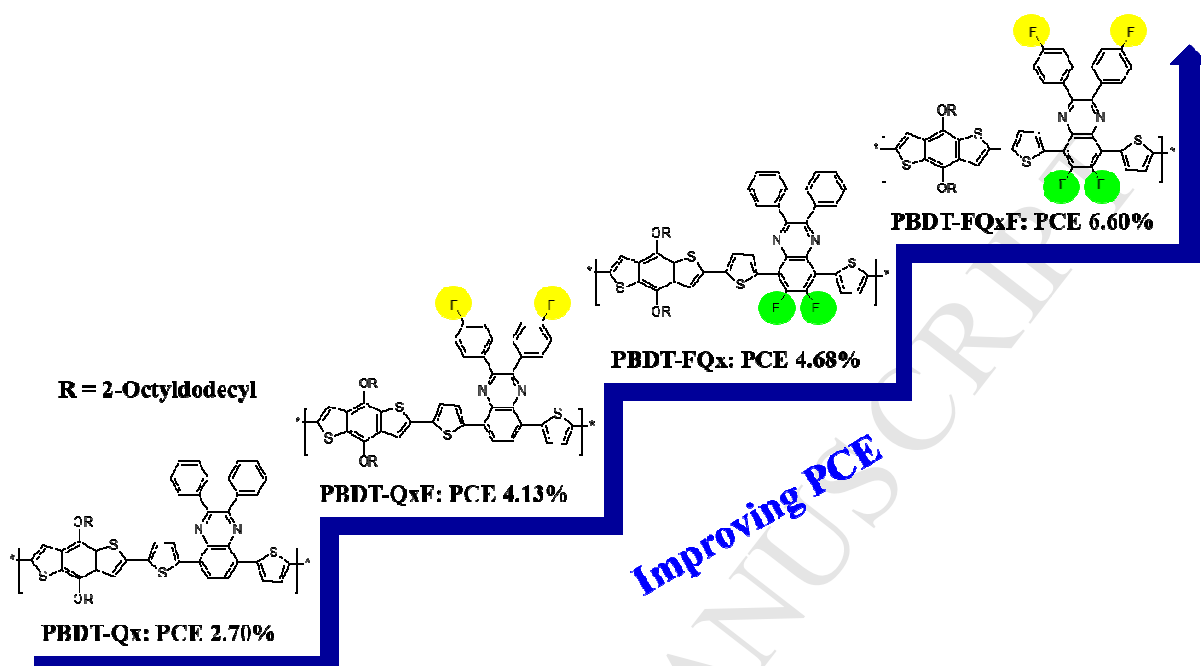


GA



Step-by-Step Improvement in Photovoltaic Properties of Fluorinated Quinoxaline-Based Low-Band-Gap Polymers

Sella Kurnia Putri,^{a†} Yun Hwan Kim,^{b†} Dong Ryeol Whang,^c Min Seok Lee,^a Joo Hyun Kim,^{*,b} and
Dong Wook Chang^{*,a}

^aDepartment of Industrial Chemistry, Pukyong National University, 48547 Pusan, Republic of Korea

^bDepartment of Polymer Engineering, Pukyong National University, 48547 Pusan, Republic of Korea

^cLinz Institute for Organic Solar Cells (LIOS)/Institute of Physical Chemistry, Johannes Kepler University Linz, 4040 Linz, Austria

Corresponding Authors

D. W. Chang: dwchang@pknu.ac.kr

J. H. Kim: jkim@pknu.ac.kr

†Author Contributions

S. K. Putri and Y. H. Kim equally contributed to this research.

Abstract

A series of fluorinated quinoxaline-based polymers with typical donor- π -acceptor configurations has been synthesized by Stille coupling reaction. The electron-donating dialkoxy-substituted benzodithiophene (**BDT**) is connected to the electron-withdrawing 2,3-diphenylquinoxaline (**DPQ**) acceptor through a thiophene bridge. To investigate the effect of strong electron-withdrawing moieties, fluorine atoms have been systematically incorporated at various positions on the DPQ units such as the 6,7-positions, the *para*-positions of the phenyl substituent on the 2,3-positions, and both locations to afford **PBDT-QxF**, **PBDT-FQx**, and **PBDT-FQxF**, respectively. Because of significant contributions from the fluorine atoms, these polymers display quite differentiated optical and electrochemical properties in comparison with those of their non-fluorinated counterpart, **PBDT-Qx**. In addition, a gradual improvement in power conversion efficiencies (PCEs) is observed in the order of **PBDT-Qx**, **PBDT-QxF**, **PBDT-FQx**, and **PBDT-FQxF**, when inverted-type polymer solar cells (PSCs) with a configuration of ITO/ZnO/polymers:PC₇₁BM/MoO₃/Al were fabricated. In particular, **PBDT-FQxF**, with four fluorine atoms on the 6,7-positions and the *para*-positions of the phenyl substituent on 2,3-positions of DPQ, exhibits the highest PCE of 6.60% with an open-circuit voltage (V_{oc}) of 0.91 V, a short-circuit current density (J_{sc}) of 10.15 mA/cm⁻², and a fill factor (FF) of 71.5%.

Keywords: Low band gap polymer; benzothiadiazole; 2,3-diphenylquinoxaline; fluorine; polymer solar cells

1. Introduction

Owing to their unique advantages such as lightweight, easy processability, and superior flexibility, polymer solar cells (PSCs) have attracted great interest during recent decades.¹⁻³ Upon formation of bulk heterojunction (BHJ) structures between conjugated polymeric electron donors and electron acceptors (mostly fullerene-based materials) in an active layer of PSCs, the charge separation and transportation of photo-generated excitons can be greatly facilitated, which enables efficient conversion from solar light to electrical energy. Unceasing and innovative efforts, including material developments and device optimizations can greatly improve the power conversion efficiency (PCE) of PSCs to more than 10 %.⁴⁻⁷

So far, many low-band-gap conjugated polymers have been intensively developed for use as photo-active components in PSCs.⁸⁻⁹ They usually possess alternating electron-donating (D) and electron-withdrawing (A) building blocks along their conjugated backbones, leading to a significant reduction in the band gap through efficient formation of intramolecular charge transfer (ICT) states. In particular, the quinoxaline moiety has recently attracted great attentions as a major electron-accepting building block in low-band-gap polymers, because of its unique advantages such as high electron affinity, simple preparation, and structural versatility.¹⁰⁻¹⁶

Recently, the incorporation of an electron-withdrawing fluorine atom, especially onto electron-accepting units of conjugated polymer structures, has come to be regarded one of the more promising approaches for enhancing photovoltaic performances of PSCs.¹⁷ The high electron affinity and small size of the fluorine atom can efficiently modulate the energy levels by lowering both the lowest unoccupied molecular orbital (LUMO) and highest occupied molecular orbital (HOMO) energy level and minimizing the undesirable steric hindrance of conjugated polymers, respectively.¹⁷ Therefore, a significant improvement in PCEs to more than 8% has been obtained

from fluorinated quinoxaline-based PSCs.¹⁸⁻¹⁹ Among various quinoxaline derivatives, 2,3-diphenylquinoxaline (DPQ) is usually considered as an essential motif for introducing fluorine atoms, because of its facile preparation and structural diversity.¹⁴ For example, Chen *et al.* demonstrated a high PCE of up to 8.0% from PSCs with a 6,7-difluorinated DPQ-based low-band-gap copolymer.²⁰ Similar promising results have been observed from other polymers with mono- or difluorinated DPQ units on its 6,7-positions.²¹⁻²⁵ Apart from the 6,7-positions of DPQ, it has been also reported that the introduction of fluorine atoms on the *para*-position of phenyl ring on 2,3-positions of the DPQ moiety can significantly improve the photovoltaic properties of PSCs.²⁶⁻²⁷ Although, these results clearly underline the usefulness of fluorine atoms on diverse positions of DPQ moieties for photovoltaic applications, more studies are required to better understand the effects of fluorine substituents on the various characteristics of DPQ-based conjugated polymers.

Herein, we synthesized a series of DPQ-based low-band-gap polymers with a typical D- π -A configuration, in which an electron-donating dialkoxy-substituted benzodithiophene (BDT) was linked to electron-accepting DPQ derivatives through a thiophene linker. For systematic investigations, fluorine atoms were incorporated onto the 6,7-positions of DPQ, the *para*-positions of the phenyl substituents on the 2,3-positions of DPQ and both locations on the DPQ unit in a non-fluorinated standard polymer, **PBDT-Qx**, to afford **PBDT-QxF**, **PBDT-FQx**, and **PBDT-FQxF**, respectively (Figure 1). This simple but methodical approach enabled us to well comprehend the positional and populational influence of fluorine atoms on various aspects of DPQ-based low-band-gap polymers, including optical and electrochemical properties together with photovoltaic characteristics.

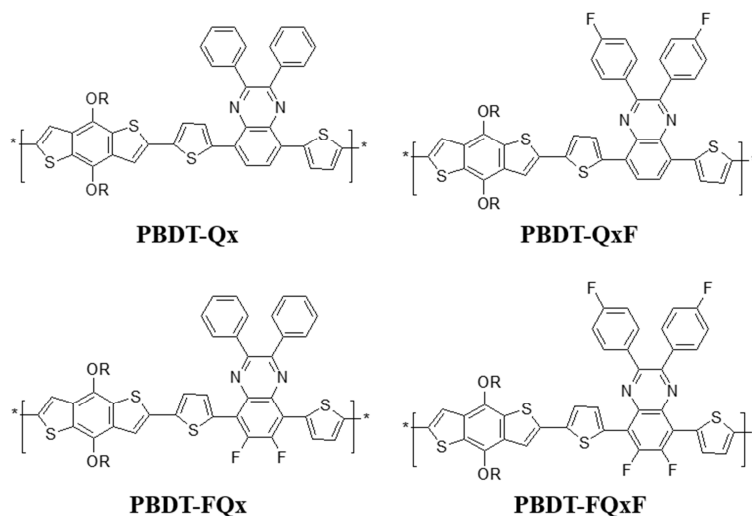


Figure 1. Chemical structures of **PBDT-Qx**, **PBDT-QxF**, **PBDT-FQx**, and **PBDT-FQxF**.

2. Experimental Section

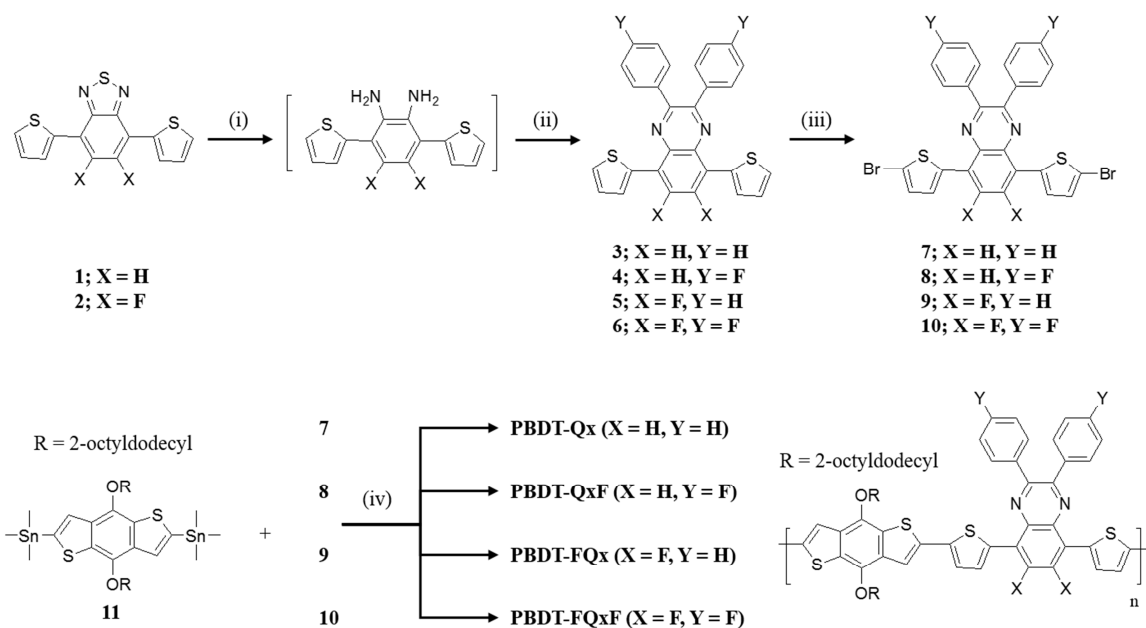
2.1. Materials and instruments

4,7-Di(thiophen-2-yl)benzo[*c*][1,2,5]thiadiazole (**1**), 5,6-difluoro-4,7-di(thiophen-2-yl)benzo[*c*][1,2,5]thiadiazole (**2**), and 2,6-bis(trimethyltin)-4,8-bis(2-octyldodecyloxy)benzo[1,2-*b*:4,5-*b'*]dithiophene (**11**) were synthesized according to the previous literatures.²⁸⁻³⁰ Benzil and 4,4'-difluorobenzil were purchased from Aldrich and TCI, respectively. All other chemicals and solvents were obtained from Aldrich Chemical Co., Inc. ¹H, ¹³C, and ¹⁹F NMR spectra were measured with a JEOL JNM ECP-400 spectrometer. UV-visible spectra were recorded on a JASCO V-530 UV-Vis spectrophotometer. Matrix-assisted laser desorption/ionization time-of-flight (MALDI-TOF) spectroscopy was conducted by using a Bruker Ultraflex spectrometer. Gel permeation chromatography (GPC) was measured on an Agilent 1200 series instrument with THF as the eluent. Cyclic voltammetry (CV) measurements were carried out by using a VersaSTAT3 potentiostat (Princeton Applied Research) with tetrabutylammonium hexafluorophosphate (0.1 M, Bu₄NPF₆) as the electrolyte in acetonitrile. For CV measurements, a glassy carbon electrode coated with

polymers and a platinum wire were used as the working and counter electrode, respectively. A silver wire was used as a pseudo-reference electrode with a ferrocene/ferrocenium external standard. The thickness of the films was measured with an Alpha-Step IQ surface profiler (KLA-Tencor Co.), and the atomic force microscopy (AFM) topography images were taken by using a Bruker (NanoScope V) microscope operated in tapping mode.

2.2. Fabrication and analysis of photovoltaic devices

[6,6]-Phenyl C₇₁ butyric acid methyl ester (PC₇₁BM, catalog no. nano-cPCBM-SF) was obtained from Nano-C, Inc. To fabricate inverted type PSCs with indium tin oxide (ITO)/ZnO/active layer (polymer:PC₇₁BM)/MoO₃/Ag, a 25-nm-thick ZnO film was initially deposited on an ITO surface by using a sol-gel process. The partially crystalline ZnO film was prepared by thermal curing of predeposited ZnO precursors at 200 °C for 10 min. The solution of ZnO precursors was prepared by the dissolution of zinc acetate dehydrate (0.164g) and ethanolamine (0.05 ml) in methoxyethanol (1mL) and stirring the mixture for 30 min prior to film deposition. The active layer with a thickness of 80 nm was fabricated using a chloroform solution of polymeric donor and PC₇₁BM acceptor by spin-coating at 600 rpm for 60 s. Prior to spin-coating, the blended solution was filtered through a 0.2 μm polytetrafluoroethylene membrane filter. Finally, a 20-nm-thick MoO₃ layer and 100-nm-thick Ag layer were consecutively deposited by thermal evaporation at 2×10^{-6} Torr through a shadow mask with a device area of 0.13 cm². The *J-V* characteristics of device were analyzed by using a KEITHLEY Model 2400 source-measure unit under AM 1.5G illumination at 100 mW/cm² from a 150 W Xe lamp. The conditions of solar simulation were calibrated before the measurements by using a Si reference cell with a KG5 filter certified by the National Institute of Advanced Industrial Science and Technology.



Scheme 1. Synthesis of **PBTD-Qx**, **PBTD-QxF**, **PBTD-FQx** and **PBTD-FQxF**. (i) Zinc, acetic acid, 80 °C, 12 h; (ii) α -diketone, acetic acid, reflux, overnight; (iii) *N*-bromosuccinimide (NBS), RT, overnight; (iv) Pd(Ph₃)₄, toluene, 90 °C, 48 h.

2.3. Syntheses.

2.3.1. Synthesis of DPQ-based compounds 3, 4, 5 and 6

A mixture of the appropriate thiophene-attached benzothiadiazoles (**1** or **2**, 2.5 mmol) and zinc powder (20 equiv., 50 mmol) in acetic acid (60 mL) was stirred at 80 °C for 12 h. Upon completion of the reaction, the mixture was filtered to remove zinc powder and the filtrate was carefully collected. After addition of α -diketone (benzil or 4,4'-difluorobenzil, 2.5 mmol) to the filtrate, the solution was heated to reflux overnight. The solution was cooled to room temperature, and the mixture was poured into water and extracted with chloroform. The organic layers were separated,

dried over magnesium sulfate, and filtered. Solvents were removed under reduced pressure, and the crude residue was further purified by column chromatography with chloroform/ethanol (1/4, v/v).

2.3.2. 2,3-Diphenyl-5,8-di(thiophen-2-yl)quinoxaline (3)

4,7-Di(thiophene-2-yl)benzo[c]-[1,2,5]thiadiazole (**1**) and benzil were used as reactants. Yield: 62% (light green solid). ^1H NMR (400 MHz, CDCl_3): δ (ppm) = 8.17 (s, 2H), 7.89 (d, 2H, J = 3.76 Hz), 7.75 (m, 4H), 7.53 (d, 2H, J = 5.12 Hz), 7.42-7.38 (m, 6H), 7.20 (dd, 2H, J = 3.76, 5.12 Hz). ^{13}C NMR (100 MHz, CDCl_3): δ (ppm) = 154.3, 141.4, 141.3, 139.9, 133.9, 133.1, 131.7, 131.5, 130.9, 129.7, 129.3, 129.1. MALDI-TOF MS: m/z calcd, 446.586; found, 446.127 [M^+].

2.3.3. 2,3-Di(4-fluorophenyl)-5,8-di(thiophen-2-yl)quinoxaline (4)

4,7-Di(thiophene-2-yl)benzo[c]-[1,2,5]thiadiazole (**1**) and 4,4'-difluorobenzil were used as reactants. Yield: 58% (light green solid). ^1H NMR (400 MHz, CDCl_3): δ (ppm) = 8.15 (s, 2H), 7.84 (d, 2H, J = 3.76 Hz), 7.72 (dd, 4H, J = 5.36, 8.60 Hz), 7.52 (d, 2H, J = 5.12 Hz), 7.18 (dd, 2H, J = 5.12, 3.76 Hz), 7.09 (t, 4H, J = 8.60 Hz). ^{13}C NMR (100 MHz, CDCl_3): δ (ppm) = 167.1, 165.2, 154.0, 153.0, 141.2, 139.8, 135.0, 131.6, 129.9, 129.3, 129.1, 118.2, 118.1, 110.0. ^{19}F NMR (376 MHz, CDCl_3): δ (ppm) = -111.51. MALDI-TOF MS: m/z calcd, 482.567; found, 483.121 [M^+].

2.3.4. 6,7-Difluoro-2,3-diphenyl-5,8-di(thiophen-2-yl)quinoxaline (5)

5,6-Difluoro-4,7-di(thiophen-2-yl)benzo[c][1,2,5]thiadiazole (**2**) and benzil were used as reactants. Yield: 68% (yellow solid). ^1H NMR (400 MHz, CDCl_3): δ (ppm) = 8.05 (d, 2H, J = 3.76 Hz), 7.72 (m, 4H), 7.65 (d, 2H, J = 5.12 Hz), 7.41-7.37 (m, 6H), 7.22 (dd, 2H, J = 3.76, 5.12 Hz). ^{13}C NMR (100 MHz, CDCl_3): δ (ppm) = 152.2, 138.8, 135.6, 131.6, 131.5, 131.4, 131.2, 130.8, 129.9, 129.0,

127.3 ^{19}F NMR (376 MHz, CDCl_3): δ (ppm) = -128.68. Mass, m/z calcd, 482.07; found, 481.85 $[\text{M}^+]$.

2.3.5. 6,7-Difluoro-2,3-bis(4-fluorophenyl)-5,8-di(thiophen-2-yl)quinoxaline (6)

5,6-Difluoro-4,7-di(thiophen-2-yl)benzo[*c*][1,2,5]thiadiazole (**2**) and 4,4'-difluorobenzil were used as reactants. Yield: 65% (orange solid). ^1H NMR (400 MHz, CDCl_3): δ (ppm) = 8.00 (d, 2H, J = 3.76 Hz), 7.68 (dd, 4H, J = 5.36, 8.84 Hz), 7.65 (d, 2H, J = 5.12 Hz), 7.23 (dd, 2H, J = 3.76, 5.12 Hz), 7.08 (t, 4H, J = 8.84 Hz). ^{13}C NMR (125 MHz, CDCl_3): δ (ppm) = 164.3, 162.6, 150.2, 134.7, 134.0, 132.4, 132.3, 130.9, 130.5, 130.1, 126.7, 117.9, 115.7, 115.5. ^{19}F NMR (376 MHz, CDCl_3): δ (ppm) = -111.09, -128.18. Mass, m/z calcd, 518.55; found, 517.85 $[\text{M}^+]$.

2.3.6. Synthesis of dibromo-DPQ compounds 7, 8, 9, 10

A mixture of the appropriate DPQ compound (**3**, **4**, **5**, **6**; 1.0 mmol) and *N*-bromosuccinimide (NBS; 2.2 mmol) in THF (30 mL) was stirred at room temperature for 12 h. The reaction mixture was poured into water and extracted with ethyl acetate. The organic layers were separated, dried over magnesium sulfate and filtered. Solvents were removed under reduced pressure, and the crude residue was further purified by recrystallization from ethyl acetate/ethanol (1/4, v/v).

2.3.7. 5,8-Di(5-bromothiophen-2-yl)-2,3-diphenylquinoxaline (7)

3 was used as the starting material. Yield: 72% (orange solid). ^1H NMR (400 MHz, CDCl_3): δ (ppm) = 8.12 (s, 2H), 7.71 (m, 4H), 7.59 (d, 2H, J = 2.68 Hz), 7.44-7.40 (m, 6H), 7.14 (d, 2H, J = 2.68 Hz). ^{13}C NMR (100 MHz, CDCl_3): δ (ppm) = 154.8, 153.9, 142.2, 140.8, 139.2, 133.2, 133.1, 131.9, 130.9, 128.3, 128.2, 119.8. MALDI-TOF MS: m/z calcd, 604.378; found, 603.993 $[\text{M}^+]$.

2.3.8. 5,8-Di(5-bromothiophen-2-yl)-2,3-bis(4-fluorophenyl)quinoxaline (8)

4 was used as the starting material. Yield: 65% (light red solid). ^1H NMR (400 MHz, CDCl_3): δ (ppm) = 8.09 (s, 2H), 7.68 (dd, 4H, J = 5.36, 8.88 Hz), 7.55 (d, 2H, J = 4.32 Hz), 7.13-7.09 (m, 6H). ^{13}C NMR (100 MHz, CDCl_3): δ (ppm) = 167.0, 165.3, 153.5, 142.0, 139.2, 136.7, 135.0, 133.2, 131.8, 128.5, 119.9, 118.3, 118.2. ^{19}F NMR (376 MHz, CDCl_3): δ (ppm) = -111.02. MALDI-TOF MS: m/z calcd, 640.359; found, 639.992 [M^+].

2.3.9. 5,8-Di(5-bromothiophen-2-yl)-6,7-difluoro-2,3-diphenylquinoxaline (9)

5 was used as the starting material. Yield: 75% (orange solid). ^1H NMR (400 MHz, CDCl_3): δ (ppm) = 7.76 (d, 2H, J = 4.28 Hz), 7.65 (m, 4H), 7.42-7.37 (m, 6H), 7.13 (d, 2H, J = 4.28 Hz). ^{13}C NMR (100 MHz, CDCl_3): δ (ppm) = 152.6, 138.3, 135.1, 133.1, 131.8, 131.7, 131.6, 131.2, 130.1, 130.0, 129.1, 119.7. ^{19}F NMR (376 MHz, CDCl_3): δ (ppm) = -128.36. Mass, m/z calcd, 640.36; found, 639.55 [M^+].

2.3.10. 5,8-Di(5-bromothiophen-2-yl)-6,7-difluoro-2,3-bis(4-fluorophenyl)quinoxaline (10)

6 was used as the starting material. Yield: 70% (orange solid). ^1H NMR (400 MHz, CDCl_3): δ (ppm) = 7.78 (d, 2H, J = 4.04 Hz), 7.64 (dd, 4H, J = 5.36, 8.84 Hz), 7.17 (d, 2H, J = 4.04 Hz), 7.11 (t, 4H, J = 8.60 Hz). ^{13}C NMR (100 MHz, CDCl_3): δ (ppm) = 164.4, 162.8, 150.7, 134.2, 133.5, 132.4, 132.2, 131.2, 131.1, 129.5, 119.0, 115.8, 115.7. ^{19}F NMR (376 MHz, CDCl_3): δ (ppm) = -110.59, -127.90. Mass, m/z calcd, 676.34; found, 675.60 [M^+].

2.3.11. Synthesis of DPQ-based polymers by palladium-catalyzed Stille reaction

In a Schlenk flask, BDT monomer (0.25 mmol), dibrominated DPQ-based monomer (0.25 mmol) and Pd(PPh₃)₄ (3 mol%) were dissolved in dry toluene (10 ml). After N₂ had been bubbled through for 15 min, the reaction mixture was heated to 90 °C and vigorously stirred for 2 d under a N₂ atmosphere and then 2-trimethylstannylthiophene and 2-bromothiophene were consecutively added as end-capping agents with an interval of 3 h. Once polymerization was complete, the mixture was cooled to room temperature and poured into methanol. The precipitated black solids were collected and further purified by Soxhlet extraction with methanol, acetone, hexane, and chloroform. The polymers in the chloroform fraction were recovered by precipitation into methanol again. Finally, the polymer was dried in a vacuum oven at 50 °C.

2.3.12. PBDT-Qx

11 and **7** were used as reactants. Yield: 83% (deep purple solid). ¹H NMR (400 MHz, CDCl₃): δ (ppm) = 8.02-7.72 (br, 8H), 7.65-7.36 (br, 6H), 7.24-7.15 (br, 2H), 7.10-6.95 (br, 2H), 4.27-3.92 (br, 4H), 2.01-1.83 (br, 2H), 1.81-1.22 (br, 64H), 1.20-1.01 (br, 12H). Molecular weight by GPC: number-average molecular weight (M_n) = 49.22 KDa, polydispersity index (PDI) = 2.64. Elemental analysis: calcd (%) for C₇₈H₉₈N₂O₂S₄: C 76.55, H 8.07, N 2.29, S 10.48; found: C 76.08, H 8.15, N 2.31, S 10.57.

2.3.13. PBDT-QxF

11 and **8** were used as reactants. Yield: 80% (deep purple solid). ¹H NMR (400 MHz, CDCl₃): δ (ppm) = 8.12-7.65 (br, 10H), 7.48-7.32 (br, 2H), 7.23-7.01 (br, 4H), 4.27-3.95 (br, 4H), 2.01-1.83 (br, 2H), 1.81-1.22 (br, 64H), 1.20-1.01 (br, 12H). Molecular weight by GPC: M_n = 38.30 KDa,

PDI = 3.01. Elemental analysis: calcd (%) for $C_{78}H_{96}F_2N_2O_2S_4$: C 74.36, H 7.68, N 2.22, S 10.18; found: C 74.16, H 7.84, N 2.16, S 10.23.

2.3.14. PBDT-FQ_x

1 and **9** were used as reactants. Yield: 85% (deep purple solid). 1H NMR (400 MHz, $CDCl_3$): δ (ppm) = 8.21-7.85 (br, 4H), 7.82-7.41 (br, 8H), 7.21-7.01 (br, 4H), 4.27-3.95 (br, 4H), 2.01-1.83 (br, 2H), 1.81-1.22 (br, 64H), 1.20-1.01 (br, 12H). Molecular weight by GPC: M_n = 42.88 KDa, PDI = 2.53. Elemental analysis: calcd (%) for $C_{78}H_{96}F_2N_2O_2S_4$: C 74.36, H 7.68, N 2.22, S 10.18; found: C 74.11, H 7.81, N 2.24, S 10.22.

2.3.15. PBDT-FQ_xF

11 and **10** were used as reactants. Yield: 78% (deep purple solid). 1H NMR (400 MHz, $CDCl_3$): δ (ppm) = 8.22-7.61 (br, 6H), 7.49-7.31 (br, 2H), 7.22-7.05 (br, 6H), 4.27-3.95 (br, 4H), 2.01-1.83 (br, 2H), 1.81-1.22 (br, 64H), 1.20-1.01 (br, 12H). Molecular weight by GPC: M_n = 37.09 KDa, PDI = 3.24. Elemental analysis: calcd (%) for $C_{78}H_{94}F_4N_2O_2S_4$: C 72.30, H 7.31, N 2.16, S 9.90; found: C 71.91, H 7.50, N 2.24, S 10.23.

3. Results and discussion,

3.1. Synthesis and thermal properties

The detailed synthetic routes of all monomers and polymers are outlined in Scheme 1. Firstly, 4,7-Di(thiophen-2-yl)benzo[c][1,2,5]thiadiazole (**1**), 5,6-difluoro-4,7-di(thiophen-2-yl)benzo[c][1,2,5]thiadiazole (**2**), were reduced with Zn powder to give *ortho*-diamine intermediates, which were consecutively condensed with benzil or 4,4'-difluorobenzil to produce the related DPQ

compounds of **3**, **4**, **5**, and **6**. The combination of two benzothiadiazoles and two benzils can generate four kinds of thiophene-containing DPQ derivatives with different positions and numbers of fluorine atoms in their chemical structures. Bromination of **3**, **4**, **5**, and **6** with NBS then readily afford dibrominated DPQ monomers of **7**, **8**, **9**, and **10**, respectively. In addition, the electron-donating dialkoxy-substituted BDT monomer (**11**) was prepared to construct polymers with D- π -A structures. In particular, the relatively long 2-octyldodecyloxy chains were incorporated into BDT monomer to avoid solubility problems presumably caused by the DPQ-based comonomers (**7**, **8**, **9**, and **10**) without alkyl or alkoxy chains. Finally, polymerization of **11** and the relevant DPQ comonomers (**7**, **8**, **9**, and **10**) under Stille coupling condition successfully yielded four different polymers, **PBDT-Qx**, **PBDT-QxF**, **PBDT-FQx**, and **PBDT-FQxF**, respectively. The chemical structures of all monomers and polymers were clearly confirmed by various analytical techniques, and these polymers display good solubility in common organic solvents such as chloroform, THF, and toluene. GPC measurements with THF as the eluent exhibit the relatively high number-average molecular weights of 49.22, 38.30, 42.88, and 37.09 kDa for **PBDT-Qx**, **PBDT-QxF**, **PBDT-FQx**, and **PBDT-FQxF**, respectively, with corresponding polydispersity index (PDI) values of 2.64, 3.01, 2.53, and 3.24. Thermogravimetric analysis (TGA) of all polymers at a heating rate of 10 °C/min under a N₂ atmosphere were carried out, and the results are shown in Figure 2. All polymers showed good thermal stability with a similar high onset of decomposition temperature of around 320 °C at 5 wt % loss (T_{d5%}). However, no discernible thermal transitions of polymers were detected during the cooling and heating processes of differential scanning calorimetry (DSC) measurements in the temperature range from 25 to 250 °C (Figure S1 in the electronic supporting information (ESI)), due to the amorphous nature of the polymers.

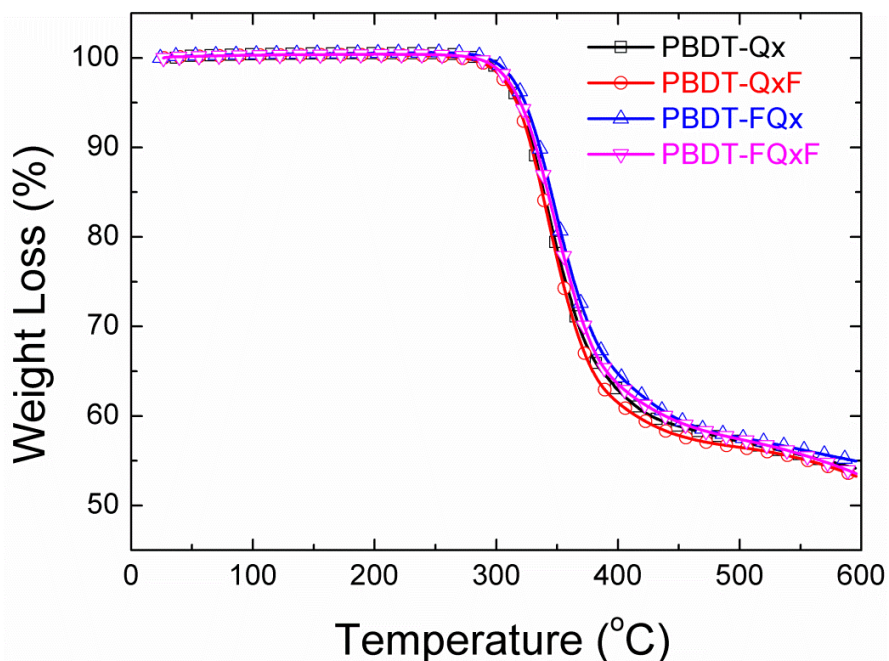


Figure 2. TGA thermograms of **PBDT-Qx**, **PBDT-QxF**, **PBDT-FQx** and **PBDT-FQxF** at a heating rate of 10 °C/min under N₂.

3.2. Optical and electrochemical properties

As shown in Figure 3a, the UV-Vis spectra of the polymer films exhibit two broad absorption bands in the shorter wavelength region (350-470 nm) and longer wavelength region (500-750 nm), respectively. The absorption band at shorter and longer wavelength region correspond to the π - π^* transition of the polymer and to the intermolecular charge transfer (ICT), respectively, which is characteristic of conjugated polymers comprising donor- π -acceptor architecture. The positions of absorption bands of the polymer films are more red-shifted than those of the solutions (Figure S2) owing to increased intermolecular interactions in the solid state. As summarized in Table 1, the absorption maxima of the **PBDT-Qx**, **PBDT-QxF**, **PBDT-FQx**, and **PBDT-FQxF** film at ICT region are 624, 610, 611 and 611 nm, respectively. The optical band gaps of **PBDT-Qx**, **PBDT-QxF**, **PBDT-FQx**, and **PBDT-FQxF** figured out from the absorption edges are 1.67, 1.71, 1.73, and

1.73 eV, respectively. The absorption maximum in the longer-wavelength region and the optical band gap are blue-shifted upon an increase in the number of fluorine atoms on the DPQ unit. The absorption spectra of the polymer thin films containing fluorine atoms show shoulders in the longer-wavelength region, which is not observed in the spectrum of **PBDT-Qx**. These shoulders are attributed to intermolecular or intramolecular aggregation through F-F and F-H interactions.³¹⁻³⁴ Herein, the blue-shifted absorption maximum is not seemed to be attributed from stronger ICT. One possible reason is that fluorine atoms increase the band gap by reducing the HOMO levels of the polymers. The changes in the absorption spectra and optical band gaps clearly demonstrate the effects of fluorine atoms on the optical and electronic properties of the polymers. Similar results have been reported for other fluorine-substituted conjugated materials.^{31-32, 34-38} The molar extinction coefficients (ϵ) at the absorption maximum wavelength of the polymer solutions with fluorine atoms (Figure S2) are higher than that of **PBDT-Qx** owing to stronger ICT in fluorine-substituted polymers.

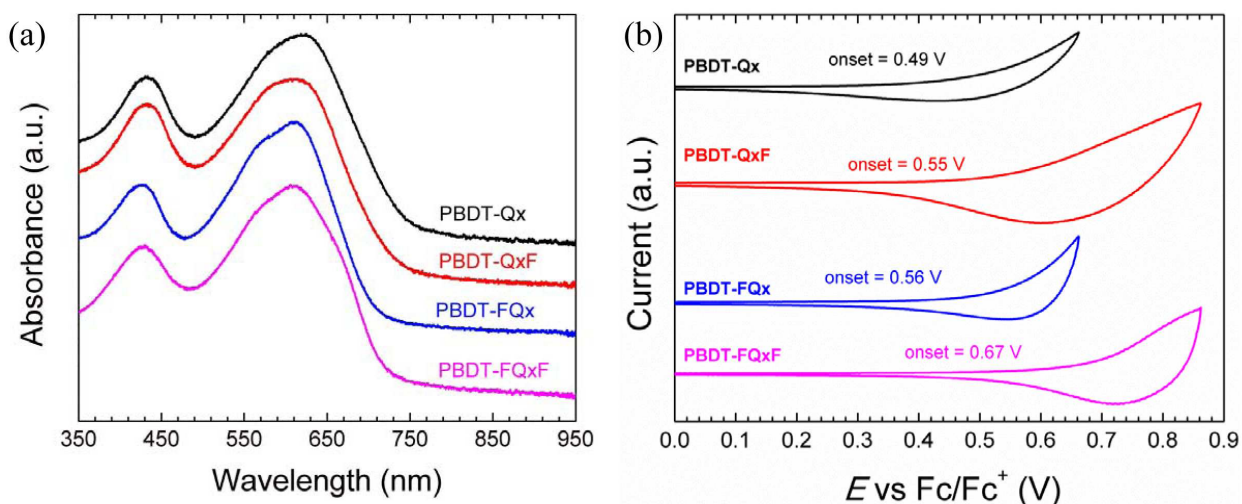


Figure 3. (a) UV-visible spectra of polymer films on glass substrate (film spectra are offset for clarity) and (b) cyclic voltammograms of polymers.

Table 1. Summary of optical and electrochemical properties of the polymers.

	$\lambda_{edge}(\text{nm})^a$	$\lambda_{max}^{film}(\text{nm})^c$	HOMO (eV) ^d	LUMO (eV) ^e
	$E_{gap}^{opt}(\text{eV})^b$			
PBDT-Qx	741	430, 624	- 5.29	- 3.62
	1.67			
PBDT-QxF	724	431, 610	- 5.35	- 3.64
	1.71			
PBDT-FQx	717	425, 611	- 5.36	- 3.63
	1.73			
PBDT-FQxF	718	426, 611	- 5.47	- 3.74
	1.73			

^aAbsorption edge of the film, ^bEstimated from the λ_{edge} , ^cMaximum wavelength of the film,

^dEstimated from the oxidation onset potential, ^eCalculated from the optical band gap and the HOMO energy level.

As shown in Figure 3b, cyclic voltammetry (CVs) measurements of the polymers show irreversible oxidation processes. The HOMO energy levels of the polymers were estimated from the oxidation onset potential of the CV measurements. The HOMO energy levels of **PBDT-Qx**, **PBDT-QxF**, **PBDT-FQx**, and **PBDT-FQxF** are -5.29, -5.35, -5.36 and -5.47 eV, respectively. With an increase in the number of substituted fluorine atoms, the HOMO levels become deeper due to the strong electronegativity of fluorine. The LUMO energy level of **PBDT-Qx**, **PBDT-QxF**, **PBDT-FQx**, and **PBDT-FQxF** were determined from the HOMO energy levels and the optical band gaps as -3.62, -3.64, -3.63, and -3.74 eV, respectively. Energy level diagrams of the polymers, PC₇₁BM,

and other materials in the device are illustrated in Figure 4. In this device configuration, facile exciton dissociation from the polymer and PC₇₁BM as well as an energetically favored charge transfer process, can efficiently take place.

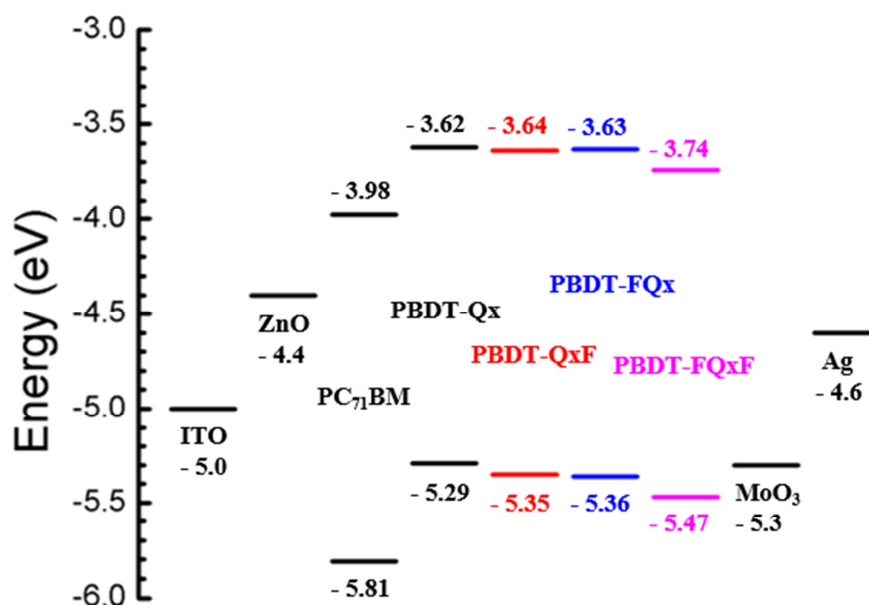


Figure 4. Energy level diagrams of polymers and materials in this research.

3.3. Theoretical calculations

The density functional theory (DFT) at the B3LP/6-31G** level was carried out with the Gaussian 09 program to explore the electronic structures of the DPQ-based low-band-gap polymers. For simple computational calculation, the 2-octyldecyl side chains on the BDT unit and the long polymer backbones were replaced with methyl groups and two repeating units, respectively. To obtain optimized molecular geometries, conformational effects were carefully considered, because there are two possible conformers with respect to the quinoxaline unit and adjacent thiophene linkers. One is a *syn*-conformer, i.e., the nitrogen atoms in quinoxaline and the sulfur atom in thiophene face on the same direction, and the other is an *anti*-conformer, i.e., the nitrogen atoms in

quinoxaline and the sulfur atom in thiophene face opposite directions. The calculated potential energy differences between *syn*- and *anti*-conformers ($E_{\text{syn}}-E_{\text{anti}}$) for **PBDT-Qx**, **PBDT-QxF**, **PBDT-FQx**, and **PBDT-FQxF** are - 0.09, - 0.11, - 0.18, and - 0.24 eV, respectively (Figure S3 in the ESI). Therefore, the *syn*-conformation is more favored for all polymers, which agrees well with previous results.¹⁵ The frontier molecular orbitals of the two repeating units with theoretical HOMO/LUMO energy levels are shown in Figure 5. Overall, the calculated HOMO/LUMO energy levels exhibit similar trends to those observed in the UV-vis and CV experiments. In Particular, the HOMO energy levels are significantly lowered, when fluorine atoms are incorporated on the 6,7-positions of the DPQ unit. In addition, the electrons are delocalized along the chain direction at the HOMO level, while they are mostly localized in the electron-withdrawing DPQ unit at the LUMO level.

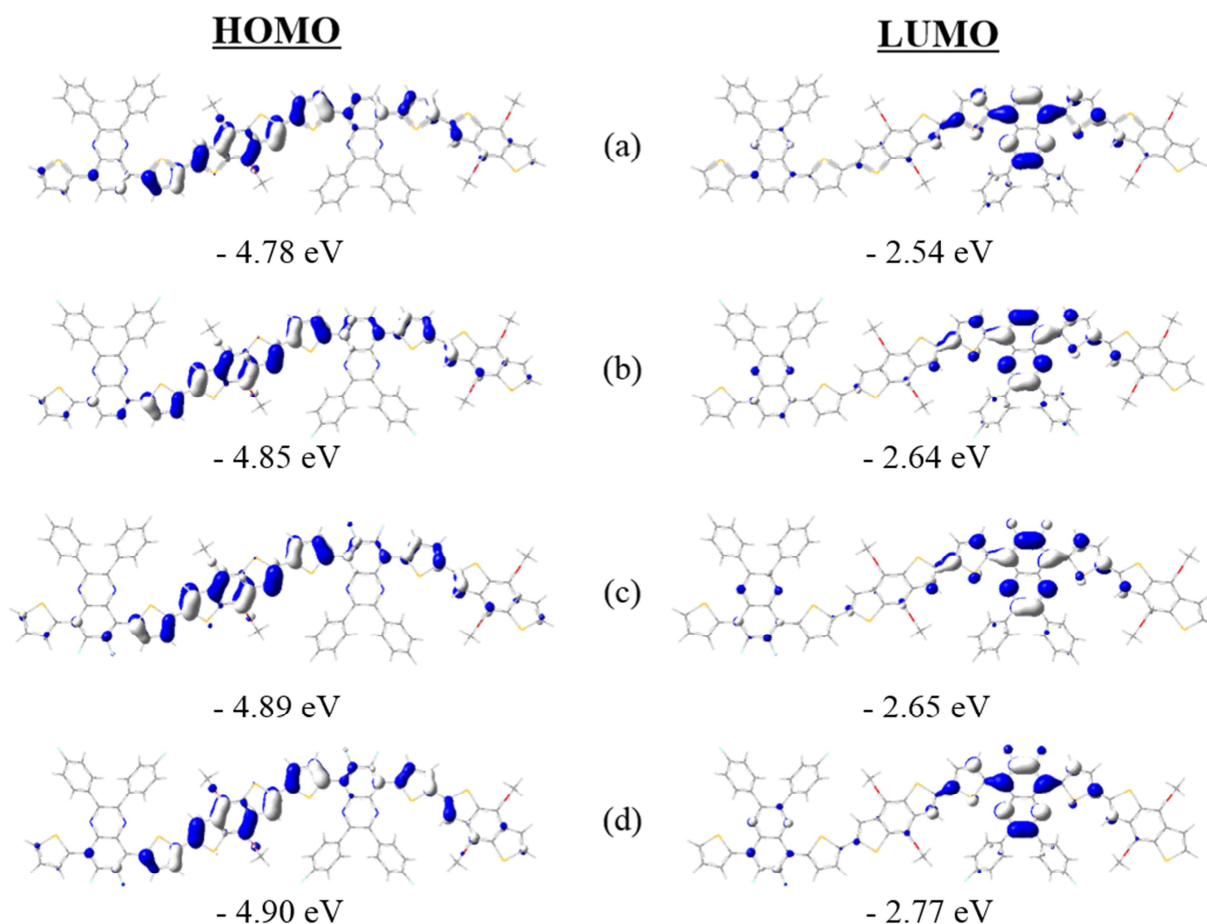


Figure 5. Frontier molecular orbitals of two-repeating unit models with HOMO/LUMO energy levels calculated at the B3LYP/6-31G** level for (a) **PBDT-Qx**, (b) **PBDT-QxF**, (c) **PBDT-FQx**, and (d) **PBDT-FQxF**.

3.4. Photovoltaic properties

In order to investigate the photovoltaic properties of the polymers, we fabricated and tested inverted type polymer solar cells (PSCs) with a structure of ITO/ZnO (40 nm)/polymer:PC₇₁BM (80 nm)/MoO₃ (10 nm)/Ag (100 nm). PSCs based on **PBDT-Qx** and **PBDT-QxF** with different blend ratios of polymers and PC₇₁BM from 3:1 to 3:9 (w/w) have been fabricated and tested to optimize the device fabrication conditions (see Table S1). In accordance with the preliminary results, we

fabricated PSCs based on a blend ratio of 3:3 (polymer: PC₇₁BM) with 1,8-diiodooctane (DIO) as a processing additive. The current density-voltage (J - V) curves at the optimized blend ratio under AM 1.5G simulated illumination are shown in Figure 6a, and the photovoltaic parameters are summarized in Table 2. In previous results, the role of fluorine atoms in conjugated polymers for photovoltaic applications were mainly focused on enhancing open-circuit voltage (V_{oc}).^{3, 39} However, concurrent increases in the short-circuit current (J_{sc}) and fill factor (FF) have also been frequently observed.^{21, 33, 35, 40-41}

Similarly, the PCEs of all polymers used in this study gradually improved with a change in the position or an increase the number of fluorine atoms, due to increasing positive contributions for all parameters including V_{oc} , J_{sc} , and FF . The devices based on the polymers with fluorine substituents, **PBDT-QxF**, **PBDT-FQx**, and **PBDT-FQxF** showed PCEs of 4.52%, 5.56%, and 6.60%, respectively, which are significantly higher than that of the non-fluorinated **PBDT-Qx** (3.14%). The V_{oc} values of the devices fabricated with **PBDT-QxF**, **PBDT-FQx**, and **PBDT-FQxF** are 0.78, 0.82, and 0.91 V, respectively, which show 27.9%, 34.4%, and 49.2% increase relative to the device based on **PBDT-Qx** (0.61 V). These gradual enhancements in V_{oc} are attributed to the deeper HOMO energy levels of the polymers, cause by incorporated fluorine atoms at different positions and with different numbers in their chemical structures. The J_{sc} data of the devices based on **PBDT-QxF**, **PBDT-FQx**, and **PBDT-FQxF** are -8.76, -9.62, and -10.15 mA/cm², respectively, which also indicate 8.4%, 19.1%, and 25.6% increases compared with that of the **PBDT-Qx** based device (-8.08 mA/cm²). The change of the J_{sc} data of the devices under 1.0 sun illumination showed very good agreement with the incident photon-to-current efficiency (IPCE; Figure 6b) curves. The IPCE data at 400-700 nm of the devices based on the polymers of **PBDT-QxF**, **PBDT-FQx**, and **PBDT-FQxF** are higher than that of the device fabricated with **PBDT-Qx**. The series resistance (R_s) data

were obtained from the inverse slope at high current regime of J - V curves in the dark (inset of Figure 6a). As shown in Table 2, the R_s data showed smaller values upon an increase in the number of fluorine atoms and agreed well with the J_{sc} and FF values.

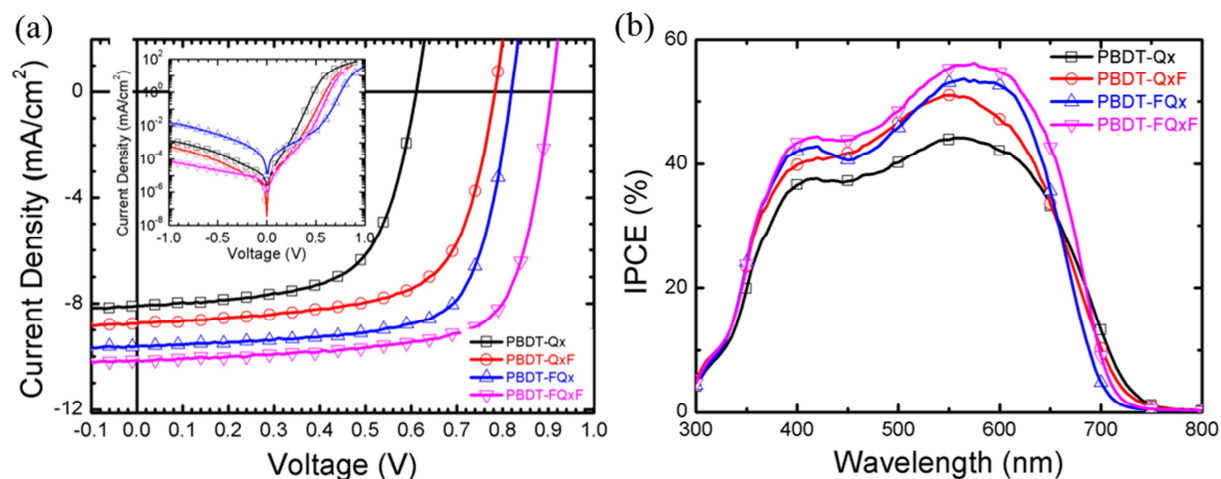


Figure 6. (a) Current density vs. voltage curves of PSCs under 1.0 sun condition (inset: under the dark condition) and (b) IPCE spectra of PSCs based on **PBDT-Qx** (square), **PBDT-QxF** (circle), **PBDT-FQx** (triangle) and **PBDT-FQxF** (inverted triangle).

Table 2. The best photovoltaic parameters of the PSCs. The averages for the photovoltaic parameters of each device are given in parentheses.

	J_{sc} (mA/cm ²)	V_{oc} (V)	FF (%)	PCE (%)	R_s (Ω cm ²) ^a
PBDT-Qx	8.08	0.61	63.7	3.14	4.02
	(7.87 ± 0.19)	(0.61 ± 0.00)	(63.1 ± 0.5)	(3.05 ± 0.07)	
PBDT-QxF	8.76	0.78	66.1	4.52	3.60
	(8.57 ± 0.11)	(0.78 ± 0.00)	(66.0 ± 0.1)	(4.42 ± 0.06)	
PBDT-FQx	9.62	0.82	70.5	5.56	2.59
	(9.49 ± 0.13)	(0.82 ± 0.00)	(70.2 ± 0.3)	(5.46 ± 0.08)	
PBDT-FQxF	10.15	0.91	71.5	6.60	2.27
	(9.97 ± 0.09)	(0.91 ± 0.00)	(71.6 ± 0.4)	(6.49 ± 0.07)	

^aSeries resistance estimated from the corresponding best device.

Electron- and hole- only devices with a structure of ITO/PEDOT:PSS (35 nm)/ polymer:PC₇₁BM (ca. 90 nm)/Au (50 nm) and ITO/Al (50 nm)/polymer:PC₇₁BM (ca. 90 nm)/Al (100 nm), respectively, have been fabricated and tested to investigate the charge transporting properties. As shown in Figure 7a&b, the J - V curves showed a characteristic of space charge limited current (SCLC) and can be expressed by the Mott-Gurney law;⁴²

$$J = \frac{9}{8} \epsilon_0 \epsilon_r \mu \frac{E^2}{L}$$

where J is the current density, μ is the charge mobility, E is the electric field, $\epsilon_0 \epsilon_r$ is the permittivity of the active layer, and L is the thickness of the active layer. The electron mobility of the device with **PBDT-Qx**, **PBDT-QxF**, **PBDT-FQx**, and **PBDT-FQxF** are 2.5×10^{-3} , 2.9×10^{-3} , 2.6×10^{-3} , and 2.4×10^{-3} cm²V⁻¹s⁻¹, respectively. Notably, the electron mobility of the polymers with or without

fluorine atoms are almost identical. The hole mobility of the devices with **PBDT-Qx**, **PBDT-QxF**, **PBDT-FQx**, and **PBDT-FQxF** are 6.95×10^{-4} , 8.67×10^{-4} s⁻¹, 9.83×10^{-4} and 9.86×10^{-4} cm²V⁻¹s⁻¹, respectively. These results indicate an increased hole mobility upon fluorination. The ratios of hole and electron mobility of the polymers with fluorine atoms are higher than that of the device based on **PBDT-Qx**, and the highest value for **PBDT-FQxF** is displayed. SCLC results indicate why the devices based on fluorine-substituted polymers showed better J_{sc} and the FF values.

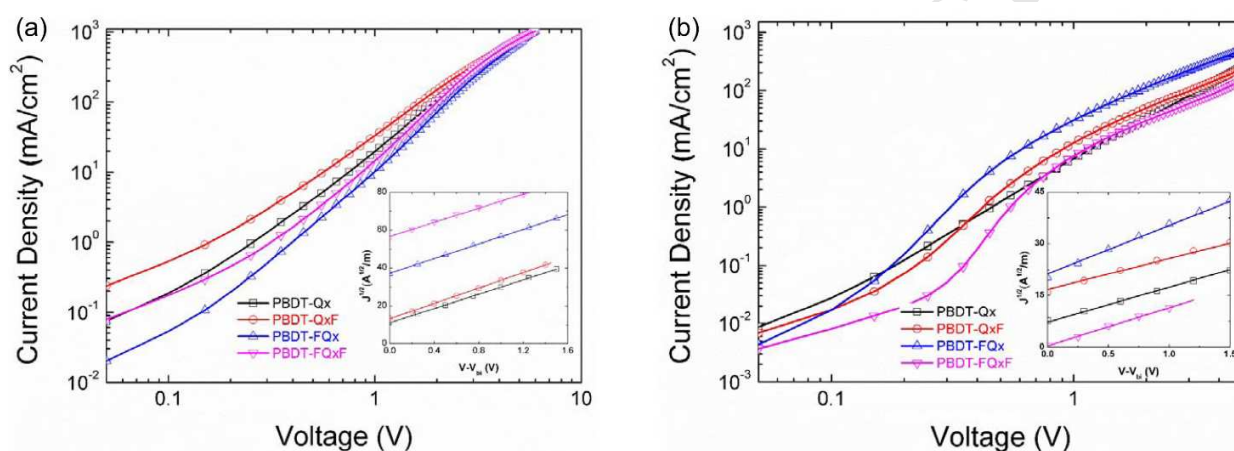


Figure 7. Current density vs. voltage curves of (a) electron- and (b) hole-only devices (inset: current density vs. voltage - built-in voltage (V_{bi}) curves with fitted lines) based on **PBDT-Qx** (square), **PBDT-QxF** (circle), **PBDT-FQx** (triangle) and **PBDT-FQxF** (inverted triangle).

Figure 8 shows the surface morphology of the active layers of the devices. The images were obtained by tapping-mode atomic force microscopy (AFM) measurements. The root-mean-squares (RMSs) of the surface of the active layers based on **PBDT-QxF**, **PBDT-FQx**, and **PBDT-FQxF** are 2.04, 1.35, 1.67 nm, respectively, which values are almost identical to that of the surface of **PBDT-Qx** (1.66 nm). The surface morphology and the RMS data hardly affect the performances of the photovoltaic devices.

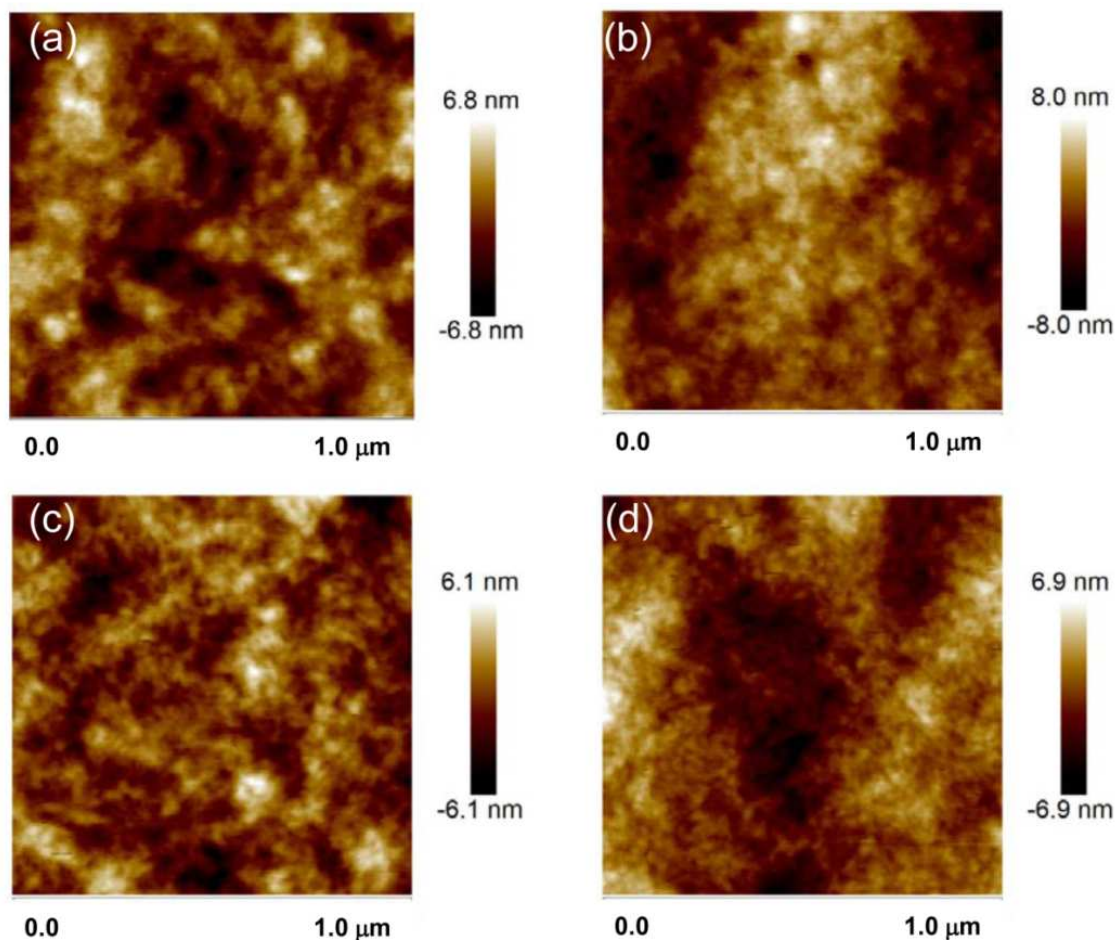


Figure 8. AFM images of the active layers based on (a) **PBDT-Qx**, (b) **PBDT-QxF**, (c) **PBDT-FQx**, and (d) **PBDT-FQxF**.

4. Conclusions

A series of fluorinated DPQ-based polymers, in which the electron-donating BDT moiety was connected with the electron-withdrawing DPQ unit through a thiophene bridge, have been synthesized by using Stille coupling reactions. Owing to the existence of two long 2-octyldodecyloxy chains on BDT, all polymers exhibited good solubility in common organic solvents. To elucidate the positional and populational effects of strong electron-withdrawing fluorine atoms on the various properties of DPQ-based polymers, fluorine atoms were

systematically incorporated into diverse positions on the DPQ unit in the polymers. Relative to the non-fluorinated counterpart of **PBDT-Qx**, the fluorinated DPQ-based polymers denoted as **PBDT-QxF**, **PBDT-FQx**, and **PBDT-FQxF** contained fluorine atoms on the 6,7-positions of DPQ, the *para*-positions of the phenyl substituents on 2,3-positions of DPQ and both locations of the DPQ unit, respectively. Optical and electrochemical investigation indicated the significant effects of fluorine atoms on the electronic properties of the polymers, such as band gaps and HOMO-LUMO energy levels. Furthermore, the gradual but noticeable improvements in the PCEs of these polymers in inverted-type PSCs were observed by increasing the number or changing the position of fluorine substituents on the DPQ unit of the polymers. Although, the PCE of non-fluorinated **PBDT-Qx** was limited to 3.14 %, enhanced PCEs of 4.52%, 5.56% and 6.60% are obtained from **PBDT-QxF**, **PBDT-FQx**, and **PBDT-FQxF**, respectively. This step-by-step enhancement in the PCEs of fluorinated DPQ-based polymers can be attributed to the positive contributions of the fluorine atoms, such as a gradual increase in V_{oc} and concomitant improvement in J_{sc} and FF through lowering of the HOMO energy levels and more balanced electron-hole mobility with smaller series resistance, respectively. Therefore, this study can provide valuable insights into the development of fluorinated conjugated polymers by careful control of structure-property relationships for various applications like photovoltaic cells and field-effect transistors.

Acknowledgements

This research work was supported by Basic Science Researches (2013R1A1A2007716, 201603930154) through the National Research Foundation (NRF) of Korea funded by the Ministry of Education, Science and Technology (MEST).

References

Supplementary data (DSC thermograms of polymers, UV-Visible spectrum of polymer solutions, optimized geometry by DFT calculation, and photovoltaic parameters of the device based on **PBDT-Qx** and **PBDT-QxF** with different blend ratios of polymers and PC₇₁BM are available in supporting information) associated with this article can be found in online

1. T. Kim, J.-H. Kim, T. E. Kang, C. Lee, H. Kang, M. Shin, C. Wang, B. Ma, U. Jeong, T.-S. Kim, Flexible, highly efficient all-polymer solar cells, *Nat. Commun* 6 (2015) 8547-8554.
2. G. Li, R. Zhu, Y. Yang, Polymer solar cells, *Nat. Photonics* 6 (2012) 153-161.S.
3. S. Gunes, H. Neugebauer, N. S. Sariciftci, Conjugated polymer-based organic solar cells, *Chem. Rev* 107 (2007) 1324-1338.
4. J. You, L. Dou, K. Yoshimura, T. Kato, K. Ohya, T. Moriarty, K. Emery, C.-C. Chen, J. Gao, G. Li, A polymer tandem solar cell with 10.6% power conversion efficiency, *Nat. Commun.* 4 (2013) 1446.
5. B. Kan, Q. Zhang, M. Li, X. Wan, W. Ni, G. Long, Y. Wang, X. Yang, H. Feng, Y. Chen, Solution-processed organic solar cells based on dialkylthiol-substituted benzodithiophene unit with efficiency near 10%, *J. Am. Chem. Soc* 136 (2014) 15529-15532.
6. Z. He, B. Xiao, F. Liu, H. Wu, Y. Yang, S. Xiao, C. Wang, T. P. Russell, Y. Cao, Single-junction polymer solar cells with high efficiency and photovoltage, *Nat. Photonics* 9 (2015) 174-179.
7. Y. Liu, J. Zhao, Z. Li, C. Mu, W. Ma, H. Hu, K. Jiang, H. Lin, H. Ade, H. Yan, Aggregation and morphology control enables multiple cases of high-efficiency polymer solar cells, *Nat. commun* 5 (2014) 5293.
8. L. Lu, T. Zheng, Q. Wu, A. M. Schneider, D. Zhao, L. Yu, Recent advances in bulk heterojunction polymer solar cells, *Chem. Rev* 115 (2015) 12666-12731.
9. Y.-J. Cheng, S.-H. Yang, C.-S. Hsu, Synthesis of conjugated polymers for organic solar cell applications, *Chem. Rev* 109 (2009) 5868-5923.
10. R. He, L. Yu, P. Cai, F. Peng, J. Xu, L. Ying, J. Chen, W. Yang, Y. Cao, Narrow-band-gap conjugated polymers based on 2,7-dioctyl-substituted dibenzo [a, c] phenazine derivatives for polymer solar cells, *Macromolecules* 47 (2014) 2921-2928.
11. L. Huo, Z. a. Tan, X. Wang, Y. Zhou, M. Han, Y. Li, Novel two-dimensional donor-acceptor conjugated polymers containing quinoxaline units: Synthesis, characterization, and photovoltaic properties, *J. Poly. Sci. A Polym. Chem* 46 (2008) 4038-4049.
12. E. Wang, L. Hou, Z. Wang, Z. Ma, S. Hellström, W. Zhuang, F. Zhang, O. Inganäs, M. R. Andersson, Side-chain architectures of 2,7-carbazole and quinoxaline-based polymers for efficient polymer solar cells, *Macromolecules* 44 (2011) 2067-2073.
13. R. Duan, L. Ye, X. Guo, Y. Huang, P. Wang, S. Zhang, J. Zhang, L. Huo, J. Hou, Application of two-dimensional conjugated benzo [1, 2-b: 4, 5-b'] dithiophene in quinoxaline-based photovoltaic polymers, *Macromolecules* 45 (2012) 3032-3038.
14. Y. Li, S.-J. Ko, S. Y. Park, H. Choi, T. L. Nguyen, M. A. Uddin, T. Kim, S. Hwang, J. Y. Kim, H. Y. Woo, A quinoxaline-thiophene based thick photovoltaic device with efficiency

- of~ 8%, *J. Mater. Chem. A* 4 (2016) 9967-9976.
15. D. Gedefaw, M. Tessarolo, W. Zhuang, R. Kroon, E. Wang, M. Bolognesi, M. Seri, M. Muccini, M. R. Andersson, Conjugated polymers based on benzodithiophene and fluorinated quinoxaline for bulk heterojunction solar cells: Thiophene versus thieno [3, 2-b] thiophene as π -conjugated spacers, *Polym. Chem* 5 (2014) 2083-2093.
 16. Y. Lee, Y. M. Nam, W. H. Jo, Enhanced device performance of polymer solar cells by planarization of quinoxaline derivative in a low-bandgap polymer, *J. Mater. Chem* 21 (2011) 8583-8590.
 17. X.-P. Xu, Y. Li, M.-M. Luo, Q. Peng, Recent progress towards fluorinated copolymers for efficient photovoltaic applications, *Chin. Chem. Lett* 27 (2016) 1241-1249.
 18. D. Liu, W. Zhao, S. Zhang, L. Ye, Z. Zheng, Y. Cui, Y. Chen, J. Hou, Highly efficient photovoltaic polymers based on benzodithiophene and quinoxaline with deeper homo levels, *Macromolecules* 48 (2015) 5172-5178.
 19. J. Yuan, L. Qiu, Z. Zhang, Y. Li, Y. He, L. Jiang, Y. Zou, A simple strategy to the side chain functionalization on the quinoxaline unit for efficient polymer solar cells, *Chem. Commun* 52 (2016) 6881-6884.
 20. H.-C. Chen, Y.-H. Chen, C.-C. Liu, Y.-C. Chien, S.-W. Chou, P.-T. Chou, Prominent short-circuit currents of fluorinated quinoxaline-based copolymer solar cells with a power conversion efficiency of 8.0%, *Chem. Mater* 24 (2012) 4766-4772.
 21. P. Yang, D. Zeigler, K. Bryant, T. Martin, D. Gamelin, C. K. Luscombe, Materials chemistry c, *J. Mater. Chem* 100 (2014) 3278-3284.
 22. J.-H. Kim, J. B. Park, H. U. Kim, I.-N. Kang, D.-H. Hwang, High open-circuit voltage organic photovoltaic cells fabricated using semiconducting copolymers consisting of bithiophene and fluorinated quinoxaline or triazole derivatives, *Synth. Met* 194 (2014) 88-96.
 23. X. Xu, Y. Wu, J. Fang, Z. Li, Z. Wang, Y. Li, Q. Peng, Side chain engineering of benzodithiophene-fluorinated quinoxaline low bandgap copolymers for high performance polymer solar cells, *Chem. Eur. J* 20 (2014) 13259-13271.
 24. X. Xu, K. Li, Z. Li, Y. Li, Z. Wang, Q. Peng, The enhanced performance of fluorinated quinoxaline-containing polymers by replacing carbon with silicon bridging atoms on the dithiophene donor skeleton, *Polym. Chem* 6 (2015) 2337-2347.
 25. Q. Tao, Y. Xia, X. Xu, S. Hedström, O. Bäcke, D. I. James, P. Persson, E. Olsson, O. Inganäs, L. Hou, D-a1-d-a2 copolymers with extended donor segments for efficient polymer solar cells, *Macromolecules* 48 (2015) 1009-1016.
 26. Q. Fan, Y. Liu, H. Jiang, W. Su, L. Duan, H. Tan, Y. Li, J. Deng, R. Yang, W. Zhu, Fluorination as an effective tool to increase the photovoltaic performance of indacenodithiophene-alt-quinoxaline based wide-bandgap copolymers, *Org. Electron* 33 (2016) 128-134.
 27. C.-P. Chen, Y.-C. Chen, C.-Y. Yu, Increased open circuit voltage in a fluorinated quinoxaline-based alternating conjugated polymer, *Polym. Chem* 4 (2013) 1161-1166.
 28. L. Liao, L. Dai, A. Smith, M. Durstock, J. Lu, J. Ding, Y. Tao, Photovoltaic-active dithienosilole-containing polymers, *Macromolecules* 40 (2007) 9406-9412.
 29. J. Kim, M. H. Yun, G.-H. Kim, J. Lee, S. M. Lee, S.-J. Ko, Y. Kim, G. K. Dutta, M. Moon, S. Y. Park, Synthesis of pcdtbt-based fluorinated polymers for high open-circuit voltage in organic photovoltaics: Towards an understanding of relationships between polymer energy levels engineering and ideal morphology control, *ACS Appl. Mater. interfaces* 6 (2014)

- 7523-7534.
30. K. W. Song, T. H. Lee, E. J. Ko, K. H. Back, D. K. Moon, Polymer solar cells based on quinoxaline and dialkylthienyl substituted benzodithiophene with enhanced open circuit voltage, *J. Poly. Sci. A Polym. Chem* 52 (2014) 1028-1036.
 31. S. A. DiBenedetto, A. Facchetti, M. A. Ratner, T. J. Marks, Molecular self-assembled monolayers and multilayers for organic and unconventional inorganic thin-film transistor applications, *Adv. Mater* 21 (2009) 1407-1433.
 32. L. Yang, J. R. Tumbleston, H. Zhou, H. Ade, W. You, Disentangling the impact of side chains and fluorine substituents of conjugated donor polymers on the performance of photovoltaic blends, *Energy Environ. Sci* 6 (2013) 316-326.
 33. Y. Zhang, S.-C. Chien, K.-S. Chen, H.-L. Yip, Y. Sun, J. A. Davies, F.-C. Chen, A. K.-Y. Jen, Increased open circuit voltage in fluorinated benzothiadiazole-based alternating conjugated polymers, *Chem. Commun* 47 (2011) 11026-11028.
 34. S. K. Putri, M. S. Lee, D. W. Chang, J. H. Kim, Fluorinated benzothiadiazole-based small molecules for photovoltaic applications, *Synth. Met* 220 (2016) 455-461.
 35. H. Zhou, L. Yang, A. C. Stuart, S. C. Price, S. Liu, W. You, Development of fluorinated benzothiadiazole as a structural unit for a polymer solar cell of 7% efficiency, *Angew. Chem. Int. Ed* 123 (2011) 3051-3054.
 36. S. C. Price, A. C. Stuart, L. Yang, H. Zhou, W. You, Fluorine substituted conjugated polymer of medium band gap yields 7% efficiency in polymer– fullerene solar cells, *J. Am. Chem. Soc* 133 (2011) 4625-4631.
 37. Y. Liang, D. Feng, Y. Wu, S.-T. Tsai, G. Li, C. Ray, L. Yu, Highly efficient solar cell polymers developed via fine-tuning of structural and electronic properties, *J. Am. Chem. Soc* 131 (2009) 7792-7799.
 38. F. Wu, Z. Deng, C. Li, L. Chen, Y. Chen, Structure evolution of fluorinated conjugated polymers based on benzodithiophene and benzothiadiazole for photovoltaics, *J. Phys. Chem. C* 119 (2015) 8038-8045.
 39. P. Heremans, D. Cheyns, B. P. Rand, Strategies for increasing the efficiency of heterojunction organic solar cells: Material selection and device architecture, *Acc. Chem. Res* 42 (2009) 1740-1747.
 40. F. Wu, D. Zha, L. Chen, Y. Chen, Photovoltaics of donor-acceptor polymers based on benzodithiophene with lateral thiophenyl and fluorinated benzothiadiazole, *J. Poly. Sci. A Polym. Chem* 51 (2013) 1506-1511.
 41. B. C. Schroeder, R. S. Ashraf, S. Thomas, A. J. White, L. Biniek, C. B. Nielsen, W. Zhang, Z. Huang, P. S. Tuladhar, S. E. Watkins, Synthesis of novel thieno [3, 2-b] thienobis (silolothiophene) based low bandgap polymers for organic photovoltaics, *Chem. Commun* 48 (2012) 7699-7701.
 42. A. Bagui, S. S. K. Iyer, Increase in hole mobility in poly (3-hexylthiophene-2, 5-diyl) films annealed under electric field during the solvent drying step, *Org. Electron* 15 (2014) 1387-1395.

Electronic Supplementary Information (ESI) for:**Step-by-Step Improvement in Photovoltaic Properties of Fluorinated Quinoxaline-Based Low-Band-Gap Polymers**

Sella Kurnia Putri,^a Yun Hwan Kim,^b Dong Ryeol Whang,^c Min Seok Lee,^a Joo Hyun Kim,^{*,b} and Dong Wook Chang^{*,a}

^aDepartment of Industrial Chemistry, Pukyong National University, 48547 Pusan, Republic of Korea

^bDepartment of Polymer Engineering, Pukyong National University, 48547 Pusan, Republic of Korea

^cLinz Institute for Organic Solar Cells (LIOS)/Institute of Physical Chemistry, Johannes Kepler University Linz, 4040 Linz, Austria

S. K. Putri and Y. H. Kim equally contributed to this research.

Corresponding Authors:

D. W. Chang: dwchang@pknu.ac.kr

J. H. Kim: jkim@pknu.ac.kr

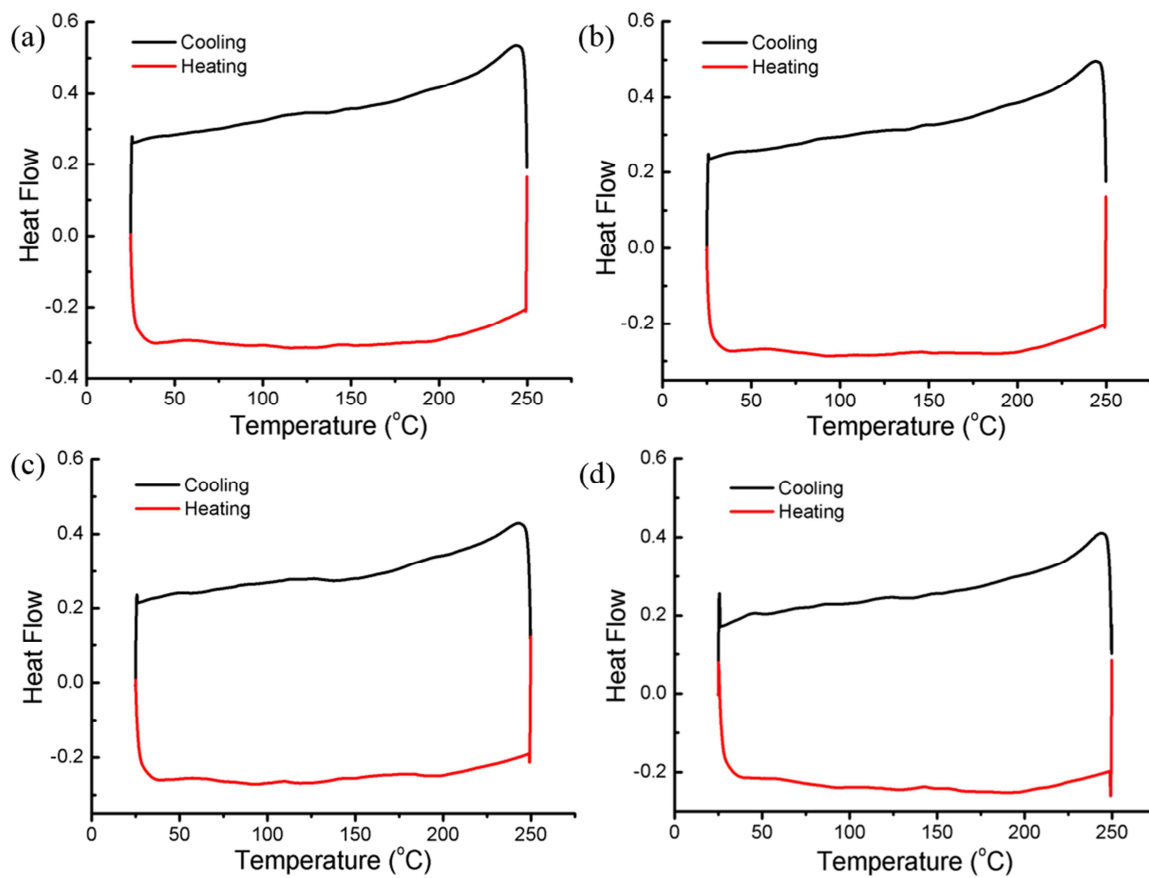


Figure S1. First cooling and second heating DSC thermograms of polymers with cooling and heating rate of 10 °C/min under N₂: (a) **PBDT-QX**; (b) **PBDT-QxF**; (c) **PBDT-FQx**; (d) **PBDT-FQxF**.

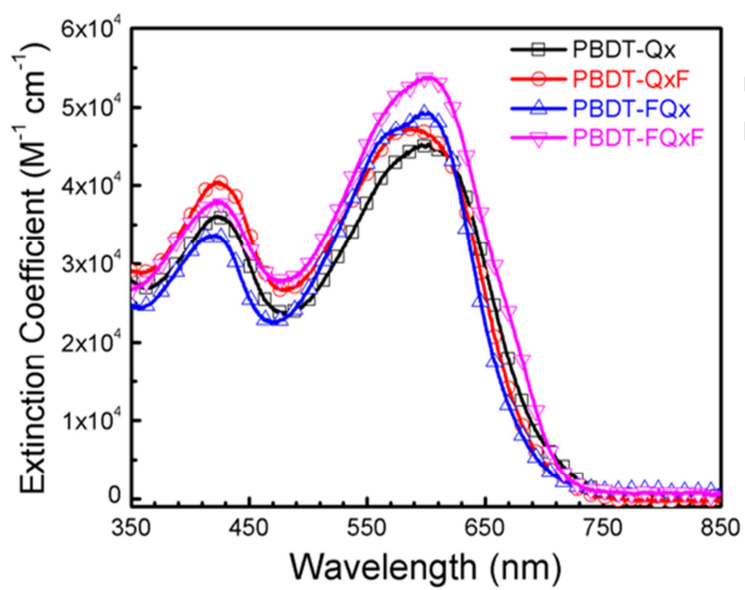


Figure S2. UV-visible spectra of all polymers in chlorobenzene.

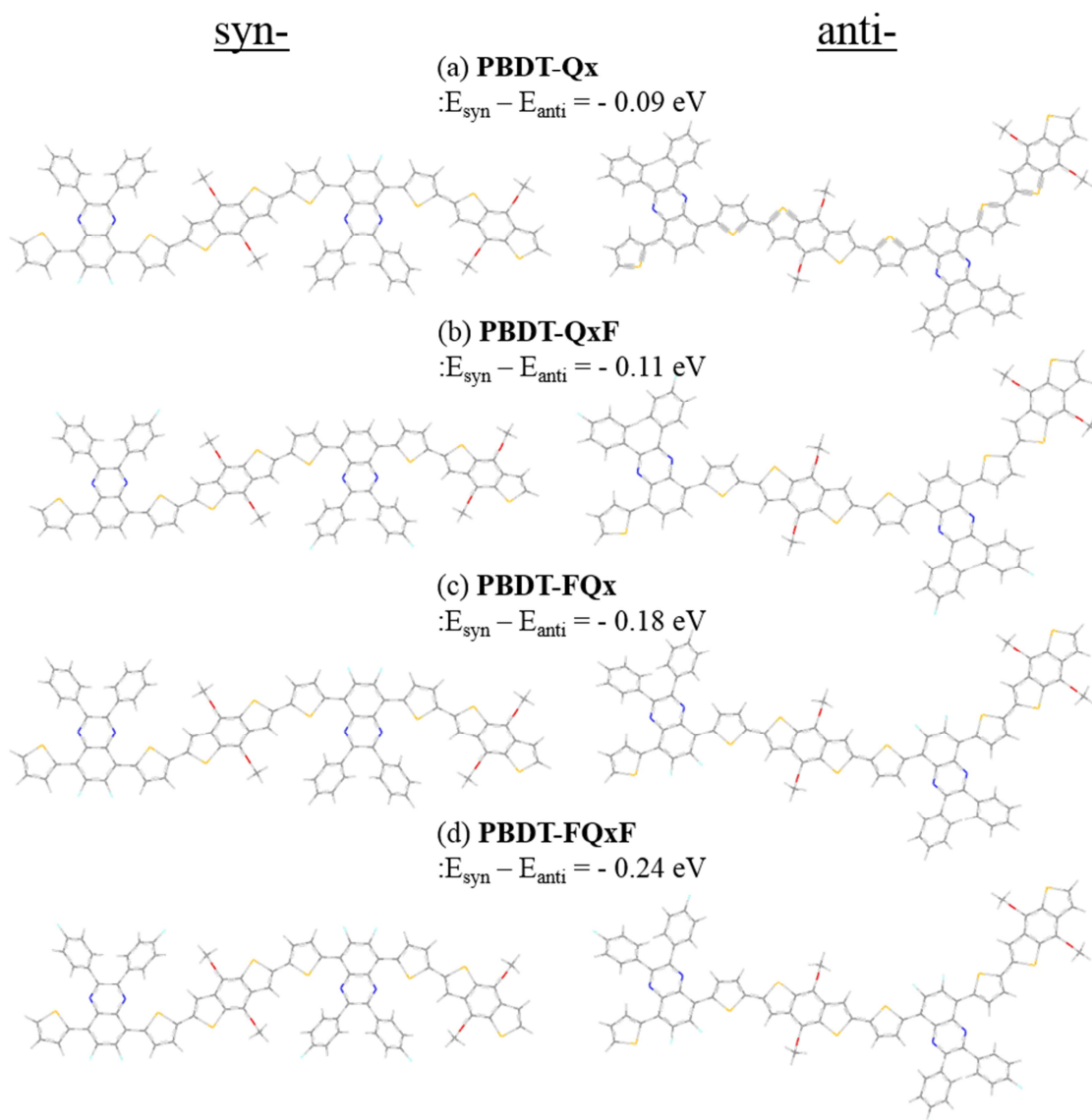


Figure S3. Optimized geometries of the two repeating unit models of the DPQ-based polymers with a syn- and anti- configuration obtained by DFT calculation.

Table S1. The best photovoltaic parameters of PSCs. The averages for the photovoltaic parameters of each device are given in parentheses.

Donor	Blend ratio^a	J_{sc} (mA/cm²)	V_{oc} (V)	FF (%)	PCE (%)	R_s (Ω cm²)^b
PBDT-Qx	3:2	7.62 (7.33 ± 0.21)	0.62 (0.62 ± 0.00)	61.8 (62.1 ± 0.4)	2.92 (2.82 ± 0.07)	-
	3:3	8.08 (7.87 ± 0.19)	0.61 (0.61 ± 0.00)	63.7 (63.1 ± 0.5)	3.14 (3.05 ± 0.07)	4.02
	3:4	8.36 (8.31 ± 0.06)	0.61 (0.61 ± 0.00)	62.7 (63.0 ± 0.6)	3.20 (3.18 ± 0.02)	-
	3:5	6.97 (6.72 ± 0.11)	0.59 (0.59 ± 0.00)	59.8 (60.4 ± 0.4)	2.46 (2.40 ± 0.03)	-
	3:6	6.06 (6.06 ± 0.00)	0.59 (0.59 ± 0.00)	60.2 (57.6 ± 2.7)	2.15 (2.06 ± 0.10)	-
	3:7.5	5.40 (5.33 ± 0.06)	0.60 (0.60 ± 0.00)	58.1 (58.0 ± 0.1)	1.88 (1.86 ± 0.02)	-
	3:9	4.47 (4.43 ± 0.05)	0.60 (0.60 ± 0.00)	52.2 (52.2 ± 0.1)	1.40 (1.37 ± 0.01)	-
	3:2	6.60 (6.59 ± 0.01)	0.80 (0.80 ± 0.00)	63.6 (63.6 ± 0.1)	3.35 (3.35 ± 0.00)	-
	3:3	8.76 (8.57 ± 0.11)	0.78 (0.78 ± 0.00)	66.1 (66.0 ± 0.1)	4.52 (4.42 ± 0.06)	3.60
	3:4	9.02 (8.87 ± 0.09)	0.77 (0.77 ± 0.00)	64.2 (64.3 ± 0.5)	4.46 (4.39 ± 0.05)	-
3:5	7.89	0.78	63.9	3.93	-	

		(7.84 ± 0.07)	(0.78 ± 0.00)	(63.5 ± 0.5)	(3.87 ± 0.05)	
		5.80	0.77	60.9	2.72	
	3:7	(5.61 ± 0.12)	(0.77 ± 0.00)	(61.6 ± 0.8)	(2.67 ± 0.04)	-
PBDT-FQx	3:3	9.62	0.82	70.5	5.56	2.59
		(9.49 ± 0.13)	(0.82 ± 0.00)	(70.2 ± 0.3)	(5.46 ± 0.08)	
PBDT-FQxF	3:3	10.15	0.91	71.5	6.60	2.27
		(9.97 ± 0.09)	(0.91 ± 0.00)	(71.6 ± 0.4)	(6.49 ± 0.07)	

^aMass ratio of donor to PC₇₁BM, ^bSeries resistance, respectively (estimated from the corresponding best device).

Highlights

- A series of low band gap polymers based on quinoxaline have been synthesized
- Selective incorporation of fluorine atoms on the quinoxaline acceptors
- Optical, electrochemical and photovoltaic properties have been investigated